
RL-SPH: Learning to Achieve Feasible Solutions for Integer Linear Programs

Tae-Hoon Lee

KAIST, Republic of Korea
 th.lee@kaist.ac.kr

Min-Soo Kim

KAIST, Republic of Korea
 minsoo.k@kaist.ac.kr

Abstract

Integer linear programming (ILP) is widely utilized for various combinatorial optimization problems. Primal heuristics play a crucial role in quickly finding feasible solutions for NP-hard ILP. Although *end-to-end learning*-based primal heuristics (E2EPH) have recently been proposed, they are typically unable to independently generate feasible solutions and mainly focus on binary variables. Ensuring feasibility is critical, especially when handling non-binary integer variables. To address this challenge, we propose RL-SPH, a novel reinforcement learning-based start primal heuristic capable of independently generating feasible solutions, even for ILP involving non-binary integers. Experimental results demonstrate that RL-SPH rapidly obtains high-quality feasible solutions, achieving on average a 44 \times lower primal gap and a 2.3 \times lower primal integral compared to existing primal heuristics.

1 Introduction

The traveling salesman problem and the knapsack problem are classic examples of combinatorial optimization (CO) problems, extensively studied in operations research and computer science (Gasse et al., 2022). CO involves mathematical optimization that aims to minimize or maximize a specific objective function (Mazyavkina et al., 2021). When both the objective function and the constraints of CO are linear, the problem is referred to as linear programming (LP) (Bengio et al., 2021). Furthermore, if the variables in LP are required to take integer values, it becomes an integer linear programming (ILP) (Bertsimas & Tsitsiklis, 1997). ILP has been widely applied to real-world scenarios such as logistics (Kweon et al., 2024), vehicle routing problem (Toth & Vigo, 2002), and path planning (Zuo et al., 2020).

Since ILP is NP-hard, heuristic approaches have attracted significant attention (Berthold, 2006). Primal heuristics aim to quickly find high-quality feasible solutions without guaranteeing feasibility (Berthold, 2006), in contrast to methods that aim for optimality (Cantürk et al., 2024). Traditional primal heuristics rely heavily on expert knowledge, requiring significant manual effort (Bengio et al., 2021). Recently, ML-based primal heuristics have been proposed (Nair et al., 2020; Shen et al., 2021; Yoon, 2022; Han et al., 2023; Cantürk et al., 2024; Huang et al., 2024; Liu et al., 2025), which fall under the category of *end-to-end learning* (Bengio et al., 2021; Han et al., 2023; Cantürk et al., 2024), as they learn common patterns across ILP instances and directly generate solutions. Figure 1(a) illustrates how existing *end-to-end learning*-based primal heuristics (E2EPH) combined with ILP solvers generate feasible solutions. A trained ML model generates a *partial solution* over integer variables, which is then passed to an ILP solver (e.g., Gurobi and SCIP) to obtain a feasible solution for the sub-problem.

E2EPH combined with an ILP solver have shown the ability to efficiently find high-quality solutions by reducing the search space. Despite these advances, ensuring feasibility remains a major challenge, since inaccurate ML predictions can lead to constraint violations (Han et al., 2023; Liu et al., 2025),

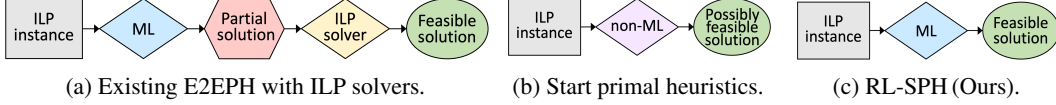


Figure 1: Comparison among E2EPH primal heuristics, start primal heuristics, and our approach.

which pose a significant obstacle to solving ILP. Recent studies (Han et al., 2023; Huang et al., 2024; Liu et al., 2025) have sought to mitigate this risk by adopting trust regions instead of strictly fixing variables (Nair et al., 2020; Yoon, 2022). However, existing E2EPH still lack the ability to independently generate feasible solutions. This limitation underscores the need for a new class of E2EPH that can independently produce feasible solutions, known as start primal heuristics.

The infeasibility caused by inaccurate ML predictions can be more pronounced for non-binary integer (hereafter, integer) variables due to their wider value range compared to binary variables. Many real-world problems such as logistics (Kweon et al., 2024), maritime transportation (Papageorgiou et al., 2014), and energy systems (Ren & Gao, 2010) involve integer variables. However, existing E2EPH studies have primarily focused on binary variables. One prior study proposed representing integer variables in binary format (Nair et al., 2020); for instance, a variable $x_i \in [0, 1000]$ is encoded as a 10-bit binary sequence, since $\lceil \log_2(1000) \rceil = 10$. However, this approach increases the dimensionality of each variable. Moreover, it is not applicable to variables with unbounded domains, which are common in practice and often the default setting in ILP solvers such as Gurobi (Gurobi Optimization, 2025) and SCIP (Bestuzheva et al., 2021). These challenges highlight the need for E2EPH techniques capable of effectively handling integer variables.

To address these challenges, we propose a novel **Reinforcement Learning-based Start Primal Heuristic**, called **RL-SPH**. Figure 1(c) illustrates how RL-SPH generates feasible solutions for ILP. Unlike existing E2EPH methods that primarily focus on binary variables, RL-SPH generates feasible solutions for ILP involving integer variables. Supervised learning approaches typically require labeled training data (e.g., near-optimal solutions), which limits their practicality for NP-hard problems (Cantürk et al., 2024). In contrast, RL-SPH operates without such data. We design a reinforcement learning framework tailored specifically to ILP, which enables the agent to learn variable-constraint relationships and achieve feasibility. Instead of directly predicting variable values, RL-SPH learns to decide whether to change the value of each integer variable. The reward functions are designed to guide the RL agent based on the degree of constraint violations and the quality of the solution. To capture long-range dependencies among variables, we adopt a Transformer-based GNN architecture.

Our main contributions are as follows.

- We propose a novel RL-based start primal heuristic, RL-SPH, which learns to generate high-quality feasible solutions for ILP in an end-to-end manner. To the best of our knowledge, RL-SPH is the first E2EPH method that explicitly learns feasibility for ILP.
- We design a solution search strategy that leverages a Transformer-based GNN trained via our RL framework tailored to ILP. The GNN agent acquires problem-solving capabilities by learning variable-constraint relationships through reward signals.
- We demonstrate that RL-SPH outperforms commonly used start primal heuristics across four CO benchmarks. Furthermore, RL-SPH combined with an ILP solver achieves high-quality solutions more quickly than baseline methods, even on instances of integer variables.

2 Preliminaries

2.1 Integer linear programming

Integer linear programming (ILP) is an optimization problem that minimizes or maximizes a linear objective function, while satisfying linear constraints and integrality constraints on decision variables (Bertsimas & Tsitsiklis, 1997). A standard form of an ILP instance can be formulated as follows:

$$\text{minimize } \mathbf{c}^\top \mathbf{x} \quad (1a)$$

$$\text{subject to } \mathbf{A}\mathbf{x} \leq \mathbf{b} \quad (1b)$$

$$x_i \in \mathbb{Z}, \quad \forall i \quad (1c)$$

$$l_i \leq x_i \leq u_i, \quad \forall i \quad (1d)$$

where $\mathbf{x} \in \mathbb{R}^n$ is a column vector of n decision variables, $\mathbf{c} \in \mathbb{R}^n$ is a column vector of the objective coefficients, $\mathbf{A} \in \mathbb{R}^{m \times n}$ is the constraint coefficient matrix, $\mathbf{b} \in \mathbb{R}^m$ is a column vector of the right-hand side of the constraints, and l_i/u_i denote the lower/upper bounds for each decision variable x_i . ILP aims to find an optimal solution that minimizes $obj = \mathbf{c}^\top \mathbf{x}$ (Eq. 1a), in the case of a minimization problem. A solution \mathbf{x} is said to be *feasible* if it satisfies all constraints (Eqs. 1b-1d).

All ILP problems can be transformed into the standard form (Eqs. 1a-1d) (Bertsimas & Tsitsiklis, 1997). Let \mathbf{a}_i^\top denote a row vector of a constraint, $\mathbf{A} = (\mathbf{a}_1^\top, \dots, \mathbf{a}_m^\top)$, and $\mathbf{b} = (b_1, \dots, b_m)$. An equality constraint $\mathbf{a}_i^\top \mathbf{x} = b_i$ is equivalent to two inequality constraints: $\mathbf{a}_i^\top \mathbf{x} \geq b_i$ and $\mathbf{a}_i^\top \mathbf{x} \leq b_i$. Moreover, $\mathbf{a}_i^\top \mathbf{x} \geq b_i$ is equivalent to $-\mathbf{a}_i^\top \mathbf{x} \leq -b_i$. Maximizing $\mathbf{c}^\top \mathbf{x}$ is equivalent to minimizing $-\mathbf{c}^\top \mathbf{x}$. Thus, we only address the standard form (i.e., minimization) in the following sections.

2.2 Start primal heuristics for ILP

ILP is known to be NP-hard due to its integrality constraints (Eq. 1c) (Berthold, 2006; Nair et al., 2020). As the number of integer variables increases, the computational cost grows exponentially (Floudas, 1995). LP-relaxation transforms an original ILP problem into an LP problem by removing the integrality constraints (Bertsimas & Tsitsiklis, 1997), and the resulting LP problem can be solved in polynomial time (Karmarkar, 1984; Vanderbei, 1998). Although LPs are computationally cheaper to solve, an LP-feasible solution may be infeasible for the original ILP due to the integrality constraints (Eq. 1c) (Guieu & Chinneck, 1999).

Start primal heuristics (Figure 1(b)) do not require an initial ILP-feasible solution. Instead, they typically begin with an LP-feasible solution and attempt to convert it into an ILP-feasible one (Berthold, 2006). Representative methods include diving, feasibility pump (FP), rounding, and relaxation enforced neighborhood search (RENS) (Berthold, 2006; Shoja & Axehill, 2023). Diving methods fix fractional variables in the LP solution to promising integer values and iteratively resolve the LP. FP alternates between two sequences, one LP-feasible and the other ILP-feasible, with the goal of convergence to a feasible ILP solution. Rounding methods attempt to obtain an ILP-feasible solution by rounding fractional LP values up or down. RENS constructs and solves a sub-ILP of the original problem by fixing or tightening bounds of integer variables based on the LP solution.

2.3 Bipartite graph representation of ILP

Recent studies on E2EPH represent ILP instances as bipartite graphs (Nair et al., 2020; Yoon, 2022; Han et al., 2023; Cantürk et al., 2024; Huang et al., 2024; Liu et al., 2025). In this representation, one set of nodes corresponds to constraints, and the other to decision variables. An edge connects a variable node to a constraint node if and only if the variable appears in the corresponding constraint. For example, in Figure 2(a), variable x_3 appears in constraint \mathbf{a}_2 ; thus, the node representing x_3 is connected to the node representing \mathbf{a}_2 in the bipartite graph.

2.4 Transformer for graphs

The Transformer architecture (Vaswani, 2017) has achieved remarkable success across various domains, including NLP and computer vision. Recently, considerable effort has been devoted to adapting Transformers for graph-structured data (Rong et al., 2020; Zhang et al., 2020; Ying et al., 2021; Wu et al., 2021b; Lin et al., 2022; Min et al., 2022). The attention mechanism in Transformers allows each node to attend to all other nodes, which enables the model to effectively learn relationships between distant nodes (Wu et al., 2021b).

Existing E2EPH methods commonly utilize GCN, which is based on the message passing neural network (MPNN) (Gilmer et al., 2017). MPNNs aggregate messages from the neighbor nodes, making them well-suited for capturing local structural information. However, they struggle to capture long-range dependencies between distant nodes (Zhang et al., 2020; Wu et al., 2021b). To propagate

messages between nodes that are K hops apart, an MPNN requires at least K layers. In the context of ILP, capturing relationships among variables that influence each other across multiple constraints may require deep MPNNs. Deeper architecture, however, often suffers from the oversmoothing problem (Li et al., 2018; Wu et al., 2021b; Min et al., 2022). For instance, as shown in Figure 2(a), variables x_2 and x_3 are four hops apart: $x_2 - \mathbf{a}_1 - x_1 - \mathbf{a}_2 - x_3$. Although x_2 and x_3 do not appear in the same constraint, they are indirectly connected via x_1 , which is shared by both \mathbf{a}_1 and \mathbf{a}_2 . A change in x_2 can affect x_1 , which in turn may influence x_3 . Modeling such interactions would require four GCN layers, but even shallow MPNNs with 2–4 layers are prone to oversmoothing (Wu et al., 2023). Therefore, we adopt a Transformer-based GNN, which can more effectively learn relationships among distant variables.

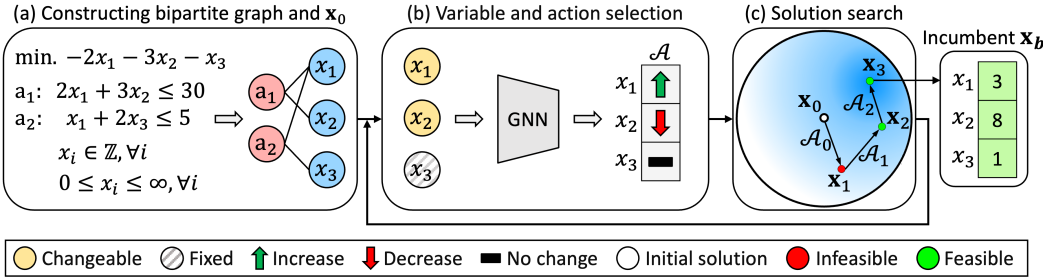


Figure 2: The overview of the RL-SPH method.

3 Methodology

This section presents RL-SPH in detail. Figure 2 illustrates the overall process. Given an ILP instance, RL-SPH constructs a bipartite graph and an initial solution \mathbf{x}_0 . At each timestep, it selects \tilde{n} changeable variables as input to the trained agent. The agent selects actions expected to yield high rewards and generates a new solution. As the process repeats, the best feasible solution found so far (i.e., the incumbent) \mathbf{x}_b is updated whenever \mathbf{x}_{t+1} is both feasible and improves upon \mathbf{x}_b .

3.1 Reinforcement learning for ILP

Our RL framework for ILP aims to train an agent to make decisions that maximize rewards while interacting with a given instance. Figure 3 depicts how the RL agent interacts with an ILP instance, where \mathcal{S}_t , \mathcal{A}_t , and $\mathcal{R}_{t, total}$ denote the observation, the set of selected actions, and the total reward at timestep t , respectively. The instance M serves as the environment for the agent. Using $\mathcal{A}_t = (a_{t,1}, \dots, a_{t,n})$, the agent updates the solution \mathbf{x}_{t+1} for n variables. This update affects the left-hand side of the constraints \mathbf{lhs}_{t+1} , the feasibility state vector \mathbf{f}_{t+1} , and the objective value obj_{t+1} . At the next timestep, the agent receives a new observation \mathcal{S}_{t+1} changed by its previous actions and selects a new action set \mathcal{A}_{t+1} to maximize rewards. By comparing the estimated reward with the actual reward $\mathcal{R}_{t+1, total}$ obtained from \mathcal{A}_{t+1} , the agent refines its policy π .

3.1.1 Observation

We define the observation $\mathcal{S}_t = (\mathbf{x}_t, \mathbf{f}_t, obj_t)$. The solution \mathbf{x}_t is obtained by updating variable values based on the agent’s previous actions \mathcal{A}_{t-1} . For example, if $\mathcal{A}_{t-1} = (a_{t-1,1}, a_{t-1,2}, a_{t-1,3}) = (+1, -1, +0)$, then \mathbf{x}_{t-1} in Figure 3(b) is updated to $\mathbf{x}_t = (x_{t,1}, x_{t,2}, x_{t,3}) = (4, 8, 0)$. Using the updated \mathbf{x}_t , the new $\mathbf{lhs}_t = \mathbf{Ax}_t$ and $obj_t = \mathbf{c}^\top \mathbf{x}_t$ are calculated.

Each element of \mathbf{f}_t ($= \mathbf{b} - \mathbf{lhs}_t$) indicates whether the corresponding constraint is satisfied by \mathbf{x}_t . Non-negative elements in \mathbf{f}_t indicate satisfied constraints, while negative ones indicate violations. For example, in Figure 3, \mathbf{x}_{t+1} yields $\mathbf{lhs}_{t+1} = (34, 3)$ for constraints \mathbf{a}_1 and \mathbf{a}_2 . Since $\mathbf{f}_{t+1} = \mathbf{b} - \mathbf{lhs}_{t+1} = (30, 5) - (34, 3) = (-4, 2)$, \mathbf{x}_{t+1} violates \mathbf{a}_1 but satisfies \mathbf{a}_2 .

3.1.2 Action

At timestep t , the agent selects a set of actions $\mathcal{A}_t = (a_{t,1}, \dots, a_{t,n})$ for n variables based on \mathcal{S}_t . For each variable, the agent can take one of three actions: increase, no change, or decrease, as shown in Figure 3(a). The magnitude of change for both increases and decreases is set to 1.

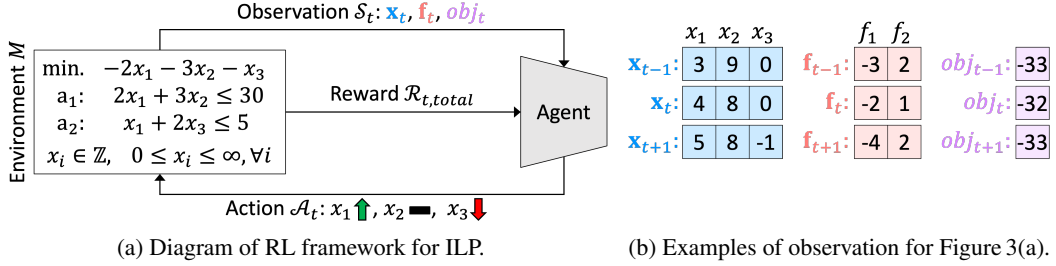


Figure 3: Reinforcement learning for ILP.

3.1.3 Reward

We design reward functions to guide the agent in selecting actions that maximize the total reward $\mathcal{R}_{t,\text{total}}$ for a given ILP instance, as follows:

$$\mathcal{R}_{t,\text{total}} = \mathcal{R}_{t,\text{opt}} + \mathcal{R}_{t,\text{explore}} \quad (2)$$

$$\mathcal{R}_{t,\text{explore}} = \begin{cases} -100, & \text{if } \mathbf{x}_{t+1} = \mathbf{x}_t, \\ 0, & \text{otherwise.} \end{cases} \quad (3)$$

To prevent premature termination of exploration, we impose a heavy penalty of -100 (Eq. 3). Finding a feasible solution is a prerequisite for improving the incumbent. Thus, our primary goal is to find a feasible solution that satisfies all constraints. The feasibility reward $\mathcal{R}_{t,\text{F}}$, used in Eqs. (7) and (8), is computed based on the variable bounds and linear constraints, as follows:

$$\mathcal{R}_{t,\text{F}} = \mathcal{R}_{t,\text{bound}} + \frac{1}{\sqrt{\tilde{n}}} \mathcal{R}_{t,\text{const}} \quad (4)$$

$$\mathcal{R}_{t,\text{bound}} = - \sum_{i=1}^n \mathbb{I}(x_{t+1,i} \notin [l_i, u_i]), \quad \mathcal{R}_{t,\text{const}} = \sum_{j=1}^m \min(f_{t+1,j}, 0) - \min(f_{t,j}, 0). \quad (5)$$

where \mathbb{I} is the indicator function, $x_{t,i}$ of \mathbf{x}_t is the value of the i -th decision variable at timestep t , $f_{t,j}$ is the element of \mathbf{f}_t for the j -th linear constraint, and \tilde{n} is the number of changeable variables. The bound reward $\mathcal{R}_{t,\text{bound}}$ imposes a penalty proportional to the number of variables that violate their bounds. For example, in Figure 3(b), $\mathcal{R}_{t,\text{bound}} = -1$ since $l_i = 0$ and $x_{t+1,3} = -1$. The constraint reward $\mathcal{R}_{t,\text{const}}$ reflects the improvement (or deterioration) for each infeasible linear constraint. For example, in Figure 3(b), $\mathcal{R}_{t,\text{const}}$ is $\{[-4 - (-2)] + \{0 - (0)\}\} = -2$.

The reward system operates in two phases: *phase1* continues until the first feasible solution is found, while *phase2* begins thereafter. The optimization reward $\mathcal{R}_{t,\text{opt}}$ is calculated, as follows:

$$\mathcal{R}_{t,\text{opt}} = \begin{cases} \mathcal{R}_{t,\text{p1}}, & \text{if agent is in } \textit{phase1}, \\ \mathcal{R}_{t,\text{p2}}, & \text{otherwise.} \end{cases} \quad (6)$$

$$\mathcal{R}_{t,\text{p1}} = \begin{cases} \mathcal{R}_{t,\text{bound}}, & \text{if } \mathcal{R}_{t,\text{const}} \geq 0 \wedge \mathbf{obj}_{t+1} < \mathbf{obj}_t \wedge (x_i \notin [l_i, u_i] \forall i), \\ \mathcal{R}_{t,\text{bound}} - \Delta \mathbf{obj}_t, & \text{if } \mathcal{R}_{t,\text{const}} \geq 0 \wedge \mathbf{obj}_{t+1} \geq \mathbf{obj}_t \wedge (x_i \notin [l_i, u_i] \forall i), \\ \mathcal{R}_{t,\text{F}} + \Delta \mathbf{obj}_t, & \text{if } \mathcal{R}_{t,\text{const}} \geq 0 \wedge \mathbf{obj}_{t+1} < \mathbf{obj}_t \wedge (x_i \in [l_i, u_i] \forall i), \\ \mathcal{R}_{t,\text{F}} - \Delta \mathbf{obj}_t, & \text{if } \mathcal{R}_{t,\text{const}} < 0 \wedge \mathbf{obj}_{t+1} \geq \mathbf{obj}_t, \\ \mathcal{R}_{t,\text{F}}, & \text{otherwise.} \end{cases} \quad (7)$$

$$\mathcal{R}_{t,\text{p2}} = \begin{cases} \Delta \mathbf{obj}_t, & \text{if } \mathbf{x}_{t+1} \in \mathcal{F} \wedge \mathbf{obj}_{t+1} < \mathbf{obj}_b, \\ -\Delta \mathbf{obj}_t \cdot \alpha, & \text{if } \mathbf{x}_{t+1} \in \mathcal{F} \wedge \mathbf{obj}_{t+1} \geq \mathbf{obj}_b, \\ \mathcal{R}_{t,\text{F}}, & \text{if } \mathbf{x}_{t+1} \notin \mathcal{F} \wedge \mathbf{obj}_{t+1} < \mathbf{obj}_b, \\ \mathcal{R}_{t,\text{F}} \cdot \alpha & \text{otherwise.} \end{cases} \quad (8)$$

where \mathcal{F} is the feasible region, $\Delta \mathbf{obj}_t = |\mathbf{obj}_{t+1} - \mathbf{obj}_t| / \max(|\mathbf{c}|)$, and α is a toward-optimal bias set to two in our study. In *phase1*, the primary goal is to find the first feasible solution from an infeasible initial solution. Since improvements in constraint violations are meaningless when variable bounds are still violated, positive values of $\mathcal{R}_{t,\text{const}}$ are ignored to prioritize satisfying the bounds (Cases 1, 2

in Eq. 7). In all other cases, the agent receives the feasibility reward $\mathcal{R}_{t,F}$ during *phase1* (Cases 3, 4, 5 in Eq. 7). Achieving a better (i.e., lower) objective value in *phase1* leads to a stronger starting point for *phase2*. Accordingly, the agent receives a reward proportional to the improvement in the objective value (Cases 2, 3, 4 in Eq. 7). A well-trained agent maximizes the total reward and is thus guaranteed to discover a feasible solution, as established in Proposition 1:

Proposition 1. *Suppose $\mathbf{x}_t \notin \mathcal{F}$, $\mathcal{R}_{t,const} > 0$, and $\mathcal{R}_{t,bound} = 0$ for all $t < \mathcal{T}$. Then $\mathbf{x}_{\mathcal{T}} \in \mathcal{F}$.*

Proof. Appendix A provides the proof of Proposition 1. \square

In *phase2*, the goal is to improve the incumbent solution \mathbf{x}_b . If the agent finds $\mathbf{x}_{t+1} \in \mathcal{F}$, it receives a reward proportional to the improvement in the objective value (Cases 1, 2 in Eq. 8). If $\mathbf{x}_{t+1} \notin \mathcal{F}$, it is penalized for constraint violations (Cases 3, 4 in Eq. 8). A suitable α promotes the agent to explore promising regions where $obj_{t+1} < obj_b$. Appendix B visually explains the reward functions.

3.1.4 Learning algorithm

We adopt the Actor-Critic (AC) algorithm (Mnih et al., 2016), which has proven effective for CO problems (Bello et al., 2016; Hubbs et al., 2020; Zong et al., 2022). AC combines a policy-based actor and a value-based critic. The actor aims to maximize the expected reward by learning a policy $\pi_{\theta}(\mathcal{A} \mid \mathcal{S})$ that maps an observation \mathcal{S} to a probability distribution over actions \mathcal{A} . The critic evaluates \mathcal{S} using a value function $V_{\theta}(\mathcal{S})$.

During training, our agent begins with an initial solution obtained via either *LP-relaxation* or *random assignment*. If a more sophisticated initialization method is available, it can be readily integrated into RL-SPH. At timestep t , the agent observes \mathcal{S}_t and selects \mathcal{A}_t using $\pi_{\theta}(\mathcal{A}_t \mid \mathcal{S}_t, phase_t)$, where $phase_t$ indicates whether the agent is in *phase1* or *phase2*. Upon executing \mathcal{A}_t , the ILP environment returns the observed reward $\mathcal{R}_{t,total}$ and \mathcal{S}_{t+1} . The actor is trained to encourage actions that yield $\mathcal{R}_{t,total} > V_{\theta}(\mathcal{S}_t, phase_t)$ and to discourage those that yield lower rewards. The critic is trained to minimize the gap between \mathcal{R}_t and $V_{\theta}(\mathcal{S}_t, phase_t)$ to provide accurate feedback to the actor. To ensure sufficient training in *phase1*, the agent stays in *phase1* for a predefined number of steps, even after finding the first feasible solution. Once the step limit is reached, the agent moves on to a new instance. The full training procedure is detailed in Appendix C.

3.2 GNN architecture of the RL agent

Figure 4 shows our GNN architecture based on a Transformer encoder, comprising two components: an actor layer and a critic layer. The actor layer generates \mathcal{A}_t based on concatenated features related to decision variables, including structural information ($\mathbf{c}^T \mid \mathbf{A}$) and the current solution \mathbf{x}_t . To stabilize training, we scale $(\mathbf{c}^T \mid \mathbf{A})$ to $[-1, 1]$ using equilibration scaling (Tomlin, 1975), which normalizes each constraint by its largest absolute coefficient.

This scaling preserves problem equivalence, since multiplying a constraint by a positive scalar does not alter the solution space. From \mathbf{x}_t , we extract two features: a binary feature *bnd_lim* and the raw variable values. *bnd_lim* is set to 1 if a variable reaches or exceeds its bound, otherwise 0. For example in Figure 3, the *bnd_lim* for $x_{t,1}$, $x_{t,2}$, and $x_{t,3}$ would be 0, 0, and 1, respectively. Since the raw variable values may be unbounded, we embed them using Periodic Embedding (PE) (Gorishniy et al., 2022), which has proven effective for numerical features in ML tasks such as house price (Pace & Barry, 1997) and income prediction (Kohavi et al., 1996). PE is formulated as $PE(z) = \oplus(\sin(\tilde{z}), \cos(\tilde{z}))$, where $\tilde{z} = [2\pi w_1 z, \dots, 2\pi w_k z]$, $\oplus(\cdot)$ is concatenation, with scalar z and trainable w_i .

The critic layer approximates the expected return using a reward context composed of a phase feature $phase_t$, a PE-encoded obj_t , and a scaled \mathbf{f}_t . The reward context is essential since the total reward is calculated based on improvements in solution quality and feasibility depending on the phase (see Eq. 2). Since the two phases have distinct goals, $phase_t$ informs the agent of its current phase. We introduce *phase-separated actor* and *critic* layers to align with the different reward designs between

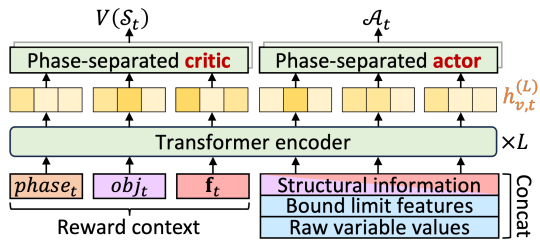


Figure 4: The GNN architecture for solving ILP.

phase1 and *phase2* as defined in Eq. 2. All other layers share parameters across both phases. \mathbf{f}_t is scaled by $\sqrt{|\mathbf{b}| + |\mathbf{b} - \mathbf{l}_{\text{hs}}|}$. To preserve shape compatibility, linear layers are applied to \mathbf{f}_t and \mathbf{A} .

3.3 Solution search strategy

Our search strategy is inspired by local search (LS), a widely used heuristic for exploring the neighborhood of a current solution for CO problems (Bertsimas & Tsitsiklis, 1997; Hillier & Lieberman, 2015). Although LS may encounter local optima, empirical studies have shown it to be effective in quickly identifying high-quality solutions (Bertsimas & Tsitsiklis, 1997). Classic LS typically perturbs a single variable at a time, whereas exploring larger neighborhoods has been shown to improve effectiveness (Shaw, 1998). In contrast to classic LS, RL-SPH allows multiple variables to change simultaneously, and thus explores a broader neighborhood. Our search strategy is similar to RENS in that it solves subproblems by fixing a set of variables. It also resembles LNS in operating over large neighborhoods; however, unlike RENS and our RL-SPH, LNS requires an initial feasible solution and is therefore difficult to use as a start primal heuristic (Berthold, 2006).

At each timestep t , RL-SPH selects $\tilde{n} = p + q$ changeable variables to explore the solution space. The selection process consists of two steps and varies by phase. In *phase1*, RL-SPH stochastically selects p seed variables that frequently appear in violated linear constraints. Then, it selects the top q neighboring variables that appear most often with the seed variables in the same constraints. For example, in Figure 3, at t , constraint \mathbf{a}_1 is infeasible, so x_1 and x_2 are candidates for selection. If $p = 1$, $q = 1$, and x_2 is selected as the seed, then x_1 , which appears in the same constraint, is selected as a neighbor. Thus, x_1 and x_2 become changeable, while x_3 remains fixed. In *phase2*, RL-SPH stochastically selects p seed variables that frequently appear in constraints with low violation risk. For instance, if $\mathbf{f}_t = (0, 5)$, then \mathbf{a}_2 has a higher probability of being selected. Neighbor selection in *phase2* follows the same procedure as in *phase1*. In our experiments, both p and q are set to $\log_2 n$, where n is the number of variables. The pseudo-code is provided in Algorithm 3, Appendix D.

Algorithm 1 outlines the overall procedure of our solution search strategy. RL-SPH first selects the variables to be changed, which are used by the actor layer π_θ to predict \mathcal{A}_t (Lines 1-2). Based on \mathcal{A}_t , the agent obtains the next observation \mathcal{S}_{t+1} (Lines 3-4). The agent receives a reward determined by the quality of \mathbf{x}_{t+1} and the degree of feasibility improvement (Line 5). If \mathbf{x}_{t+1} is a better feasible solution, both obj_b and \mathbf{x}_b are updated accordingly (Lines 6-8). To guide exploration, we restrict movement to areas where further search is unnecessary (e.g., bound violations) (Lines 9–11). In *phase1*, the agent explores freely the solution space unless variable bounds are violated (Lines 9–10). In *phase2*, movements are rolled back unless a better feasible solution is discovered (Lines 9–10). The algorithm returns $\mathcal{R}_{t,\text{total}}$, \mathcal{S}_{t+1} , \mathbf{x}_b , and obj_b for the next step (Line 12).

Algorithm 1 Solution search of RL-SPH

Input: instance M , actor layer π_θ , current observation $\mathcal{S}_t = (\mathbf{x}_t, \mathbf{f}_t, obj_t)$, incumbent solution \mathbf{x}_b and value obj_b , current phase phase_t

Output: reward $\mathcal{R}_{t,\text{total}}$, new observation \mathcal{S}_{t+1} , incumbent solution \mathbf{x}_b , and value obj_b

```

1:  $\tilde{\mathcal{S}}_t \leftarrow \text{select\_variable}(M, \mathcal{S}_t, \text{phase}_t)$  {See Algorithm 3}
2:  $\mathcal{A}_t \leftarrow \pi_\theta(\tilde{\mathcal{S}}_t, \text{phase}_t)$  {See Section 3.2}
3:  $\mathbf{x}_{t+1} \leftarrow \text{move}(\mathbf{x}_t, \mathcal{A}_t)$  {See Section 3.1.2}
4:  $\mathcal{S}_{t+1} \leftarrow \text{observe}(M, \mathbf{x}_{t+1})$  {See Section 3.1.1}
5:  $\mathcal{R}_{t,\text{total}} \leftarrow \text{reward}(M, \mathcal{S}_{t+1}, \mathcal{S}_t, obj_b, \text{phase}_t)$  {See Equation 2}
6: if  $\mathbf{x}_{t+1} \in \mathcal{F}$  and  $obj_{t+1} < obj_b$  then
7:    $obj_b \leftarrow obj_{t+1}$ 
8:    $\mathbf{x}_b \leftarrow \mathbf{x}_{t+1}$ 
9: else if ( $\text{phase}_t = 1$  and  $x_i \notin [l_i, u_i], \exists i$ ) or  $\text{phase}_t = 2$  then
10:   $\mathcal{S}_{t+1} \leftarrow \mathcal{S}_t$ 
11: end if
12: return  $\mathcal{R}_{t,\text{total}}, \mathcal{S}_{t+1}, \mathbf{x}_b, obj_b$ 

```

4 Experiments

In this section, we validate the effectiveness of RL-SPH through two experiments. First, we compare RL-SPH with existing start primal heuristics to demonstrate its ability to quickly find high-quality feasible solutions. Second, we evaluate RL-SPH combined with an ILP solver against SCIP and the existing E2EPH (Han et al., 2023), to examine whether it can reach high-quality solutions *more quickly*. Third, we conduct an ablation study to evaluate the effectiveness of each GNN component.

4.1 Experimental setup

4.1.1 Benchmarks

We conduct experiments on five NP-hard ILP benchmarks commonly used in prior works (Gasse et al., 2019; Han et al., 2023; Huang et al., 2023; Qi et al., 2021). For minimum vertex cover (MVC), we generate instances based on the Barabási-Albert random graph models (Albert & Barabási, 2002), with 3,000 nodes, yielding 3,000 variables and 11,931 constraints on average. We generate instances for independent set (IS) using the same model as MVC with 1,500 nodes. For set covering (SC) (Balas & Ho, 1980), we generate instances with 3,000 variables and 2,000 constraints. For combinatorial auction (CA) (Leyton-Brown et al., 2000), instances are generated with 4,000 items and 2,000 bids, resulting in 4,000 variables and 2,715 constraints on average. We generate instances with 2,000 integer variables and 2,000 constraints following (Qi et al., 2021), referring to as non-binary integers (NBI). For each dataset, we generated 1,000 training instances and 100 test instances. Appendix E.1 details the datasets.

4.1.2 Baselines

In the first experiment, we compare RL-SPH against four commonly used start primal heuristics, as introduced in Section 2.2: Diving, FP, Rounding, and RENS. We use the built-in implementations from the open-source ILP solver SCIP (v8.1.0), with presolving and branching disabled to isolate the heuristic performance. SCIP’s 15 diving heuristics are grouped under Diving, and its six rounding heuristics under Rounding. For each baseline, only the corresponding heuristic is enabled with default setting, while all other heuristics are disabled. Each baseline runs until its own termination condition is met, with a maximum time limit of 1,000 seconds. RL-SPH, which has no predefined termination condition, stops when all baseline methods complete their search. In the second experiment, we evaluate RL-SPH combined with SCIP (**RL-SPH+S**) against two baselines: PAS (Han et al., 2023), a representative E2EPH, combined with SCIP (**PAS+S**) and SCIP. Both SCIP and PAS+S are run with their default settings. PAS+S is trained the same duration as RL-SPH, taking around 31 minutes on IS as shown in Table 6, Appendix E.3. All randomization parameters in SCIP are set to 0 for reproducibility.

4.1.3 Metrics

We use three evaluation metrics: the *primal gap* (PG) (Huang et al., 2023; Cantürk et al., 2024), the *primal integral* (PI) (Gasse et al., 2022), and the *feasibility rate* (FR). PG quantifies how close a method’s incumbent value obj_b is to the best-known solution (BKS), and is computed as $PG(obj_b) = \frac{|obj_b - BKS|}{\max(|obj_b|, |BKS|, \epsilon)} * 100$. PI measures how quickly the incumbent improves toward BKS over time, and is defined as $PI(T) = \sum_{t=1}^T PG(obj_t)$, where $PG(obj_t) = 1$, if no feasible solution is available at timestep t . Both PG and PI are averaged only over instances where at least one feasible solution is found, and their standard deviations are reported using NumPy. FR measures the ratio of instances in which a feasible solution is obtained.

4.2 Comparison with start primal heuristics

Table 1 presents the evaluation results in terms of FR, PG, and PI, where BKS is the best objective value among all methods. RL-SPH achieved 100% FR on all benchmarks, demonstrating its effectiveness in learning feasibility. Among the baselines, only Rounding also achieved 100% FR on all benchmarks. We denote RL-SPH initialized with LP as RL-SPH(LP), and RL-SPH initialized with a randomly generated solution as RL-SPH(Random). Compared to the PG values of the baselines with 100% FR, RL-SPH(LP) achieved a 44× lower PG on average, indicating its superiority in

discovering high-quality feasible solutions. It also attained a $2.3\times$ lower PI on average, suggesting faster converges toward such solutions. Notably, RL-SPH(Random) showed comparable performance to RL-SPH(LP), which begins from an LP-feasible solution. Random initialization enables an early start, accelerating the agent’s exploration for feasible solutions without waiting for LP solving. These results suggest that RL-SPH can find feasible solutions even from less accurate initializations, and motivate the development of an initialization strategy that is more refined than random assignment but faster than LP-relaxation. RENS and Diving yield similar results on IS and MVC, as both start from the same LP-feasible solution due to the same random seed for reproducibility. Moreover, the coefficient matrix \mathbf{A} in these datasets is extremely sparse (density of 0.13% and 0.07%), resulting in LP-feasible solutions with few fractional values. In such cases, fixing variables has limited impact on the rest of the problem, leading both methods to produce similar solutions.

Table 1: Performance comparison among the start primal heuristics on four benchmarks. **Bold** and underline are used to indicate the best and second-best methods among those with 100% FR.

Dataset	Metric	Diving	FP	Rounding	RENS	RL-SPH (Ours)	
						Random	LP
IS	FR (%) \uparrow	89	100	100	89	100	100
	PG (%) \downarrow	99.98 \pm 0.05	20.60 \pm 2.10	18.09 \pm 2.74	99.98 \pm 0.05	<u>4.10</u> \pm 2.25	0.14 $^{+0.59}_{-0.14}$
	PI \downarrow	19.1 \pm 2.3	4.8 \pm 0.7	4.9 \pm 0.7	19.1 \pm 2.3	<u>3.8</u> \pm 0.4	2.5 \pm 0.2
CA	FR (%) \uparrow	100	100	100	100	100	100
	PG (%) \downarrow	90.61 \pm 1.68	18.09 \pm 9.64	<u>12.02</u> \pm 9.97	81.70 \pm 30.19	19.04 \pm 8.20	3.82 $^{+9.77}_{-3.82}$
	PI \downarrow	105.7 \pm 27.9	31.5 \pm 15.6	<u>23.0</u> \pm 15.5	112.9 \pm 27.7	36.7 \pm 14.9	21.9 \pm 13.8
SC	FR (%) \uparrow	1	99	100	3	100	100
	PG (%) \downarrow	0.00 \pm 0.00	0.34 \pm 3.11	29.98 \pm 12.38	0.00 \pm 0.00	<u>12.78</u> $^{+16.25}_{-12.78}$	9.67 $^{+15.41}_{-9.67}$
	PI \downarrow	60.0 \pm 0.0	347.5 \pm 73.5	321.5 \pm 111.0	339.3 \pm 212.8	101.3 $^{+136.7}_{-101.3}$	<u>168.0</u> \pm 124.9
MVC	FR (%) \uparrow	36	100	100	36	100	100
	PG (%) \downarrow	33.67 \pm 0.70	6.76 \pm 1.15	8.01 \pm 1.20	33.67 \pm 0.70	0.23 $^{+0.45}_{-0.23}$	<u>0.81</u> $^{+0.86}_{-0.81}$
	PI \downarrow	46.0 \pm 5.3	5.2 \pm 1.2	6.1 \pm 1.2	42.8 \pm 5.2	4.2 \pm 0.5	<u>5.0</u> \pm 0.6

4.3 Evaluation of RL-SPH combined with an ILP solver

Table 2 presents the optimization performance of the compared methods under a 50-second time limit, where *BKS* was obtained by SCIP within 1,000 seconds. RL-SPH+S fixes each variable to a unanimous value based on the feasible solutions generated by RL-SPH(LP) during the first five seconds. RL-SPH+S outperformed both SCIP and PAS+S in terms of PG and PI on both benchmarks, achieving high-quality solutions with a PG below 1% relative to the *BKS*. Unlike PAS, RL-SPH is capable of generating feasible solutions independently, allowing it to safely fix more variables using an ensemble of feasible solutions, which results in a more reduced problem size. Moreover, RL-SPH supports non-binary integer variables with a $2.3\times$ lower PI than SCIP, whereas PAS does not support such variables (NBI in Table 2). **Limitation:** Although reducing the problem size can significantly accelerate the discovery of high-quality solutions,(Nair et al., 2020), it may also introduce sub-optimality. Given that the primary goal of primal heuristics is to quickly find high-quality feasible solutions (Berthold, 2006; Cantürk et al., 2024), exact optimality is often considered a secondary concern. Nevertheless, improving the solution optimality within RL-SPH could be a promising direction for future research, as it remains an open challenge of ML for CO (Son et al., 2023).

4.4 Ablation study

Table 3 presents an ablation study on the GNN architecture, where *BKS* is defined as the best objective value among all models within a 50-second time limit. All models were trained under

Table 2: Solving performance of RL-SPH combined with an ILP solver.

Dataset	Metric	SCIP	PAS+S	RL-SPH+S	
				FR (%) \uparrow	100
IS	PG (%) \downarrow	1.24 \pm 1.01	<u>0.30</u> $^{+0.61}_{-0.30}$	0.14 \pm 0.13	
	PI \downarrow	2.4 \pm 0.3	1.7 \pm 0.4	0.5 \pm 0.5	
					100
NBI	PG (%) \downarrow	0.24 \pm 0.03	N/A	0.23 \pm 0.04	
	PI \downarrow	11.5 \pm 2.3		4.9 \pm 0.9	
					100

the same configuration using LP-feasible solutions. \emptyset showed the lowest performance on both benchmarks and notably failed to find any feasible solution on CA. With TE, the model achieved a 100% FR on both benchmarks, indicating its effectiveness in learning feasibility. Combining all components achieved the best results in PG and PI, highlighting the importance of each component.

Table 3: Ablation study on the proposed GNN architecture: RC (reward context), PSL (phase-separated layers), and TE (transformer encoder). \emptyset denotes models without all components.

Dataset	Metric	\emptyset	{RC, PSL}	{TE, PSL}	{TE, RC}	{TE, RC, PSL}
IS	FR (%) \uparrow	100	100	100	100	100
	PG (%) \downarrow	41.23 \pm 1.95	33.98 \pm 2.45	1.10 $^{+1.40}_{-1.10}$	12.93 \pm 1.96	0.62$^{+1.08}_{-0.62}$
	PI \downarrow	21.8 \pm 0.9	28.9 \pm 2.4	4.4 \pm 0.7	11.7 \pm 0.9	4.1\pm0.5
CA	FR (%) \uparrow	0	0	100	100	100
	PG (%) \downarrow	N/A	N/A	3.00 \pm 2.27	1.63 $^{+1.96}_{-1.63}$	1.20$^{+1.53}_{-1.20}$
	PI \downarrow	N/A	N/A	12.4 \pm 1.1	12.5 \pm 1.0	11.8\pm0.8

5 Related work

ML techniques for solving ILP can be broadly categorized into three groups (Bengio et al., 2021). The first group, *learning to configure algorithms*, use ML to optimize the configuration of specific components within ILP solvers. Examples include deciding parameters for promising configurations (Hutter et al., 2011), applying decomposition (Kruber et al., 2017), and selecting scaling methods (Berthold & Hendel, 2021). The second group, *ML alongside optimization algorithms*, integrates ML into ILP solvers to aid key decisions during the optimization, such as cut selection (Tang et al., 2020; Paulus et al., 2022), variable selection (Khalil et al., 2016; Alvarez et al., 2017; Gasse et al., 2019; Gupta et al., 2020; Paulus & Krause, 2023), and node selection in the branch-and-bound (He et al., 2014; Labassi et al., 2022), and neighborhood selection in LNS (Song et al., 2020; Sonnerat et al., 2021; Wu et al., 2021a; Huang et al., 2023; Liu et al., 2024).

RL-SPH belongs to the third group, *end-to-end learning*, which uses ML to directly learn and predict solutions. This group includes existing E2EPH methods (Nair et al., 2020; Shen et al., 2021; Yoon, 2022; Han et al., 2023; Cantürk et al., 2024; Huang et al., 2024; Liu et al., 2025) as well. PAS (Han et al., 2023) adopts a predefined trust region instead of strictly fixing variables, which can be viewed as the generalization of the fixing strategy (Huang et al., 2024). Recent methods (Huang et al., 2024; Liu et al., 2025) follow this approach as well. Although using trust regions alleviates the risk of infeasibility, these methods still rely on ILP solvers to obtain feasible solutions. Moreover, they do not support ILP with non-binary integer variables. To the best of our knowledge, RL-SPH is the first E2EPH method that explicitly learns to generate feasible solutions based on the theoretical foundation, even for ILP involving non-binary integers.

6 Conclusion

We proposed RL-SPH, a reinforcement learning-based start primal heuristic capable of independently generating high-quality feasible solutions for ILP. RL-SPH leverages a GNN-based RL framework to explicitly learn variable-constraint relationships, theoretically guaranteeing feasibility even from initially infeasible solutions. Experiments show RL-SPH achieves a 100% feasibility rate across five benchmarks, outperforming existing start primal heuristics with an average of 44 \times lower primal gap and 2.3 \times lower primal integral. When combined with ILP solvers, RL-SPH rapidly achieves higher-quality solutions than SCIP and PAS+SCIP. Moreover, RL-SPH naturally generalizes beyond binary variables, effectively addressing ILPs involving general integer variables.

References

Albert, R. and Barabási, A.-L. Statistical mechanics of complex networks. *Reviews of modern physics*, 74(1):47, 2002.

Alvarez, A. M., Louveaux, Q., and Wehenkel, L. A machine learning-based approximation of strong branching. *INFORMS Journal on Computing*, 29(1):185–195, 2017.

Balas, E. and Ho, A. Set covering algorithms using cutting planes, heuristics, and subgradient optimization: a computational study. *Combinatorial optimization*, pp. 37–60, 1980.

Bello, I., Pham, H., Le, Q. V., Norouzi, M., and Bengio, S. Neural combinatorial optimization with reinforcement learning. *arXiv preprint arXiv:1611.09940*, 2016.

Bengio, Y., Lodi, A., and Prouvost, A. Machine learning for combinatorial optimization: a methodological tour d’horizon. *European Journal of Operational Research*, 290(2):405–421, 2021.

Berthold, T. *Primal heuristics for mixed integer programs*. PhD thesis, Zuse Institute Berlin (ZIB), 2006.

Berthold, T. and Hendel, G. Learning to scale mixed-integer programs. In *Proceedings of the AAAI Conference on Artificial Intelligence*, volume 35, pp. 3661–3668, 2021.

Bertsimas, D. and Tsitsiklis, J. N. *Introduction to linear optimization*, volume 6. Athena Scientific Belmont, MA, 1997.

Bestuzheva, K., Besançon, M., Chen, W.-K., Chmiela, A., Donkiewicz, T., Van Doornmalen, J., Eifler, L., Gaul, O., Gamrath, G., Gleixner, A., et al. The scip optimization suite 8.0. *arXiv preprint arXiv:2112.08872*, 2021.

Cantürk, F., Varol, T., Aydoğan, R., and Özener, O. Ö. Scalable primal heuristics using graph neural networks for combinatorial optimization. *Journal of Artificial Intelligence Research*, 80:327–376, 2024.

Floudas, C. A. *Nonlinear and mixed-integer optimization: fundamentals and applications*. Oxford University Press, 1995.

Gasse, M., Chételat, D., Ferroni, N., Charlin, L., and Lodi, A. Exact combinatorial optimization with graph convolutional neural networks. *Advances in neural information processing systems*, 32, 2019.

Gasse, M., Bowly, S., Cappart, Q., Charfreitag, J., Charlin, L., Chételat, D., Chmiela, A., Du-mouchelle, J., Gleixner, A., Kazachkov, A. M., et al. The machine learning for combinatorial optimization competition (ml4co): Results and insights. In *NeurIPS 2021 competitions and demonstrations track*, pp. 220–231. PMLR, 2022.

Gilmer, J., Schoenholz, S. S., Riley, P. F., Vinyals, O., and Dahl, G. E. Neural message passing for quantum chemistry. In *Proceedings of the 34th International Conference on Machine Learning - Volume 70*, ICML’17, pp. 1263–1272. JMLR.org, 2017.

Gorishniy, Y., Rubachev, I., and Babenko, A. On embeddings for numerical features in tabular deep learning. *Advances in Neural Information Processing Systems*, 35:24991–25004, 2022.

Guieu, O. and Chinneck, J. W. Analyzing infeasible mixed-integer and integer linear programs. *INFORMS Journal on Computing*, 11(1):63–77, 1999.

Gupta, P., Gasse, M., Khalil, E., Mudigonda, P., Lodi, A., and Bengio, Y. Hybrid models for learning to branch. *Advances in neural information processing systems*, 33:18087–18097, 2020.

Gurobi Optimization, L. Gurobi optimizer reference manual. <https://docs.gurobi.com/projects/optimizer>, 2025.

Han, Q., Yang, L., Chen, Q., Zhou, X., Zhang, D., Wang, A., Sun, R., and Luo, X. A gnn-guided predict-and-search framework for mixed-integer linear programming. In *The Eleventh International Conference on Learning Representations*, 2023.

He, H., Daumé, H., and Eisner, J. Learning to search in branch and bound algorithms. *Advances in neural information processing systems*, 27, 2014.

Hillier, F. S. and Lieberman, G. J. *Introduction to operations research*. McGraw-Hill, 2015.

Huang, T., Ferber, A. M., Tian, Y., Dilkina, B., and Steiner, B. Searching large neighborhoods for integer linear programs with contrastive learning. In *International conference on machine learning*, pp. 13869–13890. PMLR, 2023.

Huang, T., Ferber, A. M., Zharmagambetov, A., Tian, Y., and Dilkina, B. Contrastive predict-and-search for mixed integer linear programs. In *Forty-first International Conference on Machine Learning*, 2024.

Hubbs, C. D., Li, C., Sahinidis, N. V., Grossmann, I. E., and Wassick, J. M. A deep reinforcement learning approach for chemical production scheduling. *Computers & Chemical Engineering*, 141: 106982, 2020.

Hutter, F., Hoos, H. H., and Leyton-Brown, K. Sequential model-based optimization for general algorithm configuration. In *Proceedings of the 5th international conference on Learning and Intelligent Optimization*, pp. 507–523, 2011.

Karmarkar, N. A new polynomial-time algorithm for linear programming. In *Proceedings of the sixteenth annual ACM symposium on Theory of computing*, pp. 302–311, 1984.

Khalil, E., Le Bodic, P., Song, L., Nemhauser, G., and Dilkina, B. Learning to branch in mixed integer programming. In *Proceedings of the AAAI conference on artificial intelligence*, volume 30, 2016.

Kohavi, R. et al. Scaling up the accuracy of naive-bayes classifiers: A decision-tree hybrid. In *Kdd*, volume 96, pp. 202–207, 1996.

Kostrikov, I. Pytorch implementations of reinforcement learning algorithms. <https://github.com/ikostrikov/pytorch-a2c-ppo-acktr-gail>, 2018.

Kruber, M., Lübecke, M. E., and Parmentier, A. Learning when to use a decomposition. In *International conference on AI and OR techniques in constraint programming for combinatorial optimization problems*, pp. 202–210. Springer, 2017.

Kweon, O., Kim, B.-I., Lee, G., Im, H., Chung, C. Y., and Lim, O. K. Parcel delivery network optimization problem considering multiple hubs and consolidation of small-sized parcels. *Computers & Industrial Engineering*, 191:110113, 2024.

Labassi, A. G., Chételat, D., and Lodi, A. Learning to compare nodes in branch and bound with graph neural networks. *Advances in neural information processing systems*, 35:32000–32010, 2022.

Leyton-Brown, K., Pearson, M., and Shoham, Y. Towards a universal test suite for combinatorial auction algorithms. In *Proceedings of the 2nd ACM conference on Electronic commerce*, pp. 66–76, 2000.

Li, Q., Han, Z., and Wu, X.-M. Deeper insights into graph convolutional networks for semi-supervised learning. In *Proceedings of the AAAI conference on artificial intelligence*, volume 32(1), 2018.

Lin, T., Wang, Y., Liu, X., and Qiu, X. A survey of transformers. *AI open*, 3:111–132, 2022.

Liu, H., Wang, J., Geng, Z., Li, X., Zong, Y., Zhu, F., Hao, J., and Wu, F. Apollo-milp: An alternating prediction-correction neural solving framework for mixed-integer linear programming. *arXiv preprint arXiv:2503.01129*, 2025.

Liu, W., Wang, A., Yang, W., and Shi, Q. Mixed-integer linear optimization via learning-based two-layer large neighborhood search. *arXiv preprint arXiv:2412.08206*, 2024.

Mazyavkina, N., Sviridov, S., Ivanov, S., and Burnaev, E. Reinforcement learning for combinatorial optimization: A survey. *Computers & Operations Research*, 134:105400, 2021.

Min, E., Chen, R., Bian, Y., Xu, T., Zhao, K., Huang, W., Zhao, P., Huang, J., Ananiadou, S., and Rong, Y. Transformer for graphs: An overview from architecture perspective. *arXiv preprint arXiv:2202.08455*, 2022.

Mnih, V., Badia, A. P., Mirza, M., Graves, A., Lillicrap, T., Harley, T., Silver, D., and Kavukcuoglu, K. Asynchronous methods for deep reinforcement learning. In Balcan, M. F. and Weinberger, K. Q. (eds.), *Proceedings of The 33rd International Conference on Machine Learning*, volume 48 of *Proceedings of Machine Learning Research*, pp. 1928–1937, New York, New York, USA, 20–22 Jun 2016. PMLR.

Nair, V., Bartunov, S., Gimeno, F., Von Glehn, I., Lichocki, P., Lobov, I., O’Donoghue, B., Sonnerat, N., Tjandraatmadja, C., Wang, P., et al. Solving mixed integer programs using neural networks. *arXiv preprint arXiv:2012.13349*, 2020.

Pace, R. K. and Barry, R. Sparse spatial autoregressions. *Statistics & Probability Letters*, 33(3):291–297, 1997.

Papageorgiou, D. J., Nemhauser, G. L., Sokol, J., Cheon, M.-S., and Keha, A. B. Mirplib—a library of maritime inventory routing problem instances: Survey, core model, and benchmark results. *European Journal of Operational Research*, 235(2):350–366, 2014.

Paulus, M. and Krause, A. Learning to dive in branch and bound. *Advances in Neural Information Processing Systems*, 36:34260–34277, 2023.

Paulus, M. B., Zarpellon, G., Krause, A., Charlin, L., and Maddison, C. Learning to cut by looking ahead: Cutting plane selection via imitation learning. In *International conference on machine learning*, pp. 17584–17600. PMLR, 2022.

Qi, M., Wang, M., and Shen, Z.-J. Smart feasibility pump: Reinforcement learning for (mixed) integer programming. *Reinforcement Learning for Real Life Workshop, International Conference on Machine Learning (ICML)*, 2021.

Ren, H. and Gao, W. A milp model for integrated plan and evaluation of distributed energy systems. *Applied energy*, 87(3):1001–1014, 2010.

Rong, Y., Bian, Y., Xu, T., Xie, W., Wei, Y., Huang, W., and Huang, J. Self-supervised graph transformer on large-scale molecular data. *Advances in neural information processing systems*, 33:12559–12571, 2020.

Shaw, P. Using constraint programming and local search methods to solve vehicle routing problems. In *International conference on principles and practice of constraint programming*, pp. 417–431. Springer, 1998.

Shen, Y., Sun, Y., Eberhard, A., and Li, X. Learning primal heuristics for mixed integer programs. In *2021 international joint conference on neural networks (ijcnn)*, pp. 1–8. IEEE, 2021.

Shoja, S. and Axehill, D. Exact complexity certification of start heuristics in branch-and-bound methods for mixed-integer linear programming. In *2023 62nd IEEE Conference on Decision and Control (CDC)*, pp. 2292–2299. IEEE, 2023.

Son, J., Kim, M., Kim, H., and Park, J. Meta-sage: Scale meta-learning scheduled adaptation with guided exploration for mitigating scale shift on combinatorial optimization. In *International Conference on Machine Learning*, pp. 32194–32210. PMLR, 2023.

Song, J., Yue, Y., Dilksina, B., et al. A general large neighborhood search framework for solving integer linear programs. *Advances in Neural Information Processing Systems*, 33:20012–20023, 2020.

Sonnerat, N., Wang, P., Ktena, I., Bartunov, S., and Nair, V. Learning a large neighborhood search algorithm for mixed integer programs. *arXiv preprint arXiv:2107.10201*, 2021.

Tang, Y., Agrawal, S., and Faenza, Y. Reinforcement learning for integer programming: Learning to cut. In *International conference on machine learning*, pp. 9367–9376. PMLR, 2020.

Tomlin, J. A. *On scaling linear programming problems*. Springer, 1975.

Toth, P. and Vigo, D. *The vehicle routing problem*. SIAM, 2002.

Vanderbei, R. J. Linear programming: foundations and extensions. *Journal of the Operational Research Society*, 49(1):94–94, 1998.

Vaswani, A. Attention is all you need. *Advances in Neural Information Processing Systems*, 2017.

Wu, X., Chen, Z., Wang, W. W., and Jadbabaie, A. A non-asymptotic analysis of oversmoothing in graph neural networks. In *The Eleventh International Conference on Learning Representations*, 2023.

Wu, Y., Song, W., Cao, Z., and Zhang, J. Learning large neighborhood search policy for integer programming. *Advances in Neural Information Processing Systems*, 34:30075–30087, 2021a.

Wu, Z., Jain, P., Wright, M., Mirhoseini, A., Gonzalez, J. E., and Stoica, I. Representing long-range context for graph neural networks with global attention. *Advances in Neural Information Processing Systems*, 34:13266–13279, 2021b.

Ying, C., Cai, T., Luo, S., Zheng, S., Ke, G., He, D., Shen, Y., and Liu, T.-Y. Do transformers really perform badly for graph representation? *Advances in neural information processing systems*, 34: 28877–28888, 2021.

Yoon, T. Confidence threshold neural diving. *NeurIPS 2021 ML4CO competition track*, 2022.

Zhang, J., Zhang, H., Xia, C., and Sun, L. Graph-bert: Only attention is needed for learning graph representations. *arXiv preprint arXiv:2001.05140*, 2020.

Zong, Z., Zheng, M., Li, Y., and Jin, D. Mapdp: Cooperative multi-agent reinforcement learning to solve pickup and delivery problems. In *Proceedings of the AAAI conference on artificial intelligence*, volume 36, pp. 9980–9988, 2022.

Zuo, Y., Tharmarasa, R., Jassemi-Zargani, R., Kashyap, N., Thiyyagalingam, J., and Kirubarajan, T. T. Milp formulation for aircraft path planning in persistent surveillance. *IEEE Transactions on Aerospace and Electronic Systems*, 56(5):3796–3811, 2020.

A Proof of Proposition 1

In this section, we prove Proposition 1:

Suppose $\mathbf{x}_t \notin \mathcal{F}$, $\mathcal{R}_{t,\text{const}} > 0$, and $\mathcal{R}_{t,\text{bound}} = 0$ for all $t < \mathcal{T}$. Then $\mathbf{x}_{\mathcal{T}} \in \mathcal{F}$.

A.1 Term definitions

- \mathcal{F} : The set of feasible solutions (feasible region) for the given original ILP problem.
- \mathbf{x}_t : The solution of the problem at timestep t .
- $\mathcal{R}_{t,\text{const}}$: The constraint reward at timestep t .
- $\mathcal{R}_{t,\text{bound}}$: The bound reward which is the sum of $\mathcal{R}_{t,\text{ub}}$ and $\mathcal{R}_{t,\text{lb}}$ at timestep t .
- $f_{t,j}$: The feasibility state for the j -th linear constraint at timestep t .
- $lhs_{t,j}$: The left-hand side of the j -th linear constraint at timestep t .
- b_j : The right-hand side of the j -th linear constraint.

A.2 Background

In our system, the action policy guarantees that the integrality requirements (Eq. 1c) are satisfied (See Section 3.1.2). Therefore, we can safely ignore the integrality constraints. In addition, since *phase1* continues until the first feasible solution is found by the definition for the phases in Section 3.1.3, we focus on satisfying the linear constraints (Eq. 1b) and the bound constraints (Eq. 1d) in *phase1*.

A.3 Proof

Suppose $\mathbf{x}_t \notin \mathcal{F}$, $\mathcal{R}_{t,\text{const}} > 0$ and $\mathcal{R}_{t,\text{bound}} = 0$.

$$\mathcal{R}_{t,\text{const}} = \sum_{j=1}^m \min(f_{t+1,j}, 0) - \min(f_{t,j}, 0) > 0$$

This implies:

$$\sum_{j=1}^m \min(f_{t,j}, 0) < \sum_{j=1}^m \min(f_{t+1,j}, 0)$$

Applying the same reasoning for time $t + 1$:

$$\sum_{j=1}^m \min(f_{t+1,j}, 0) < \sum_{j=1}^m \min(f_{t+2,j}, 0)$$

Thus, the sequence $\sum_{j=1}^m \min(f_{t,j}, 0)$ is monotonically increasing and upper-bounded by 0, which leads to:

$$\lim_{t \rightarrow \mathcal{T}} \sum_{j=1}^m \min(f_{t,j}, 0) = 0$$

Considering the $\min(\cdot)$ function at timestep \mathcal{T} , the linear constraints (Eq. 1b) satisfied as:

$$\begin{aligned} f_{\mathcal{T},j} &= b_j - lhs_{\mathcal{T},j} \geq 0, \forall j \\ lhs_{\mathcal{T},j} &\leq b_j, \forall j \\ \mathbf{A}\mathbf{x}_{\mathcal{T}} &\leq \mathbf{b} \end{aligned}$$

For $\mathcal{R}_{t,\text{bound}}$, a value of zero indicates that no decision variable violates its bounds (see Eq. 5). Hence, $\mathbf{x}_{\mathcal{T}} \in \mathcal{F}$ (i.e., $\mathbf{x}_{\mathcal{T}}$ is feasible) as long as $\mathcal{R}_{t,\text{const}} > 0$ and $\mathcal{R}_{t,\text{bound}} = 0$ in *phase1*.

B Visual explanation of reward function

B.1 Feasibility reward

The feasibility reward $\mathcal{R}_{t,F}$ is calculated in proportion to the degree of feasibility improvement or deterioration. In Figure 5, the agent violates Constraint-1 while satisfying Constraint-2. If the agent moves closer to the feasible region, it is considered an improvement in feasibility. Conversely, if it moves further away and ends up violating Constraint-2 as well, it is regarded as a deterioration. In this way, rewards are assigned based on how much the agent's actions improve or worsen feasibility. As a result, the agent learns to find feasible solutions to maximize its rewards.

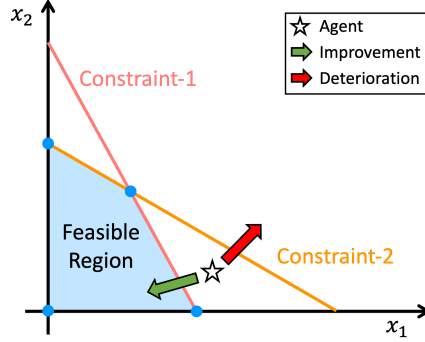


Figure 5: Illustration of feasibility improvements and deteriorations.

B.2 Reward in phase2

The green circles in Figure 6 represent better feasible solutions whose objective values is $obj_{t+1} < obj_b$ (Case 1 in Eq. 8). We regard the agent's actions that fail to find better feasible solutions than \mathbf{x}_b as incorrect (Cases 2, 3, 4). The red circle indicates a feasible solution worse than the incumbent (Case 2), while all triangles correspond to infeasible solutions (Cases 3, 4).

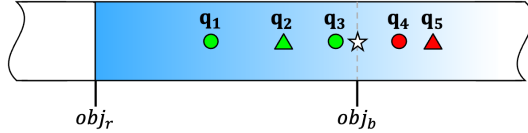


Figure 6: Illustration of reward function in *phase2*. \circ : feasible, \triangle : infeasible, green: inside, red: outside, \star : agent, obj_r : the objective value of the LP-feasible solution, obj_b : incumbent value.

Let the objective values be $obj_b = -10$, $\mathbf{q}_1 = -16$, $\mathbf{q}_2 = -13$, $\mathbf{q}_3 = -11$, $\mathbf{q}_4 = -8$, and $\mathbf{q}_5 = -7$, with $\alpha = 2$ and $\max(|\mathbf{c}|) = 1$. For the green circles, rewards in *phase2* are calculated by the first case in Eq. 8. The rewards for \mathbf{q}_1 and \mathbf{q}_3 are $\Delta obj_t = \frac{|-16 - (-10)|}{1} = 6$ and $\Delta obj_t = \frac{|-11 - (-10)|}{1} = 1$, respectively. Since \mathbf{q}_1 has the better objective value than \mathbf{q}_3 , it receives a higher reward. For the red circle, the reward is $-\Delta obj_t \cdot \alpha = -\frac{|-8 - (-10)|}{1} \cdot 2 = -4$. For the triangles, the penalties for \mathbf{q}_2 and \mathbf{q}_5 are $\mathcal{R}_{t,F}$ and $\mathcal{R}_{t,F} \cdot \alpha = 2 \cdot \mathcal{R}_{t,F}$, respectively. The distances from obj_b to \mathbf{q}_2 and \mathbf{q}_5 are the same (i.e., $|-13 - (-10)| = |-7 - (-10)| = 3$), but the penalty for \mathbf{q}_2 is smaller than that for \mathbf{q}_5 due to amplifying by α .

B.3 Toward-optimal bias

Figure 7 visualizes the agent's potential penalties by $\mathcal{R}_{t,F}$ in *phase2*. The third and fourth quadrants illustrate the penalties, assuming that $\mathcal{R}_{t,F}$ is a linear function of the gap from obj_{t+1} to the incumbent value obj_b for simplicity. As illustrated in Figures 7(a) and 7(b), a higher α results in higher penalties for solutions with $obj_{t+1} > obj_b$. By controlling the toward-optimal bias α , we can guide the agent to explore promising regions (i.e., $obj_{t+1} < obj_b$) for better feasible solutions rather than making ineffective moves (i.e., $obj_{t+1} > obj_b$), thus increasing its opportunities for learning. Appendix F provides experimental results on the toward-optimal bias α .

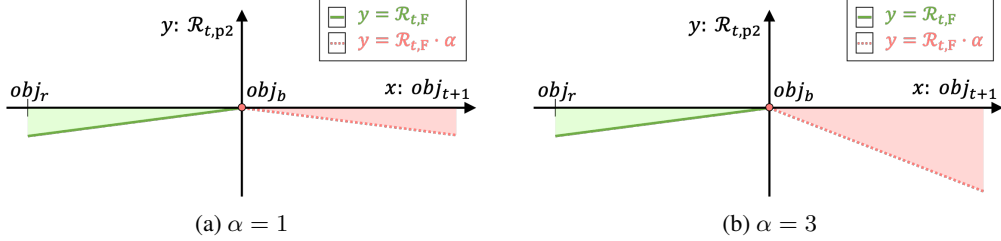


Figure 7: Illustration of the potential penalties of $\mathcal{R}_{t,p2}$ as a function of the objective value obj_{t+1} in *phase2*. The x -axis represents obj_{t+1} , and the y -axis represents $\mathcal{R}_{t,p2}$, with the origin set at obj_b .

C Pseudo-code for learning algorithm

We obtain the initial solution (Line 2) using two methods: LP-relaxation and random assignment. For LP-relaxation, we apply random rounding to the LP-feasible solution to convert the fractional variable values into integers, which may result in an infeasible solution for the original ILP problem. For random assignment, when training on the first instance, we randomly assign the value 1 to 1% of the variables. For subsequent instances, we randomly assign the value 1 to r variables, where r is half the number of variables that had the value 1 in the previous instance. Random assignment is available only for IS, CA, SC, and MVC.

Algorithm 2 Learning a policy for RL-SPH

Input: agent parameters θ , instance M
Parameter: update limit N , total step limit T_{max} , step limit for *phase1* T_{stay}
Output: updated parameters θ

```

1: for  $N$  updates do
2:    $\mathbf{x}_0 \leftarrow \text{get\_initial\_solution}(M)$ 
3:    $\mathcal{S}_0 \leftarrow \text{observe}(M, \mathbf{x}_0)$ 
4:    $\mathbf{x}_b \leftarrow \emptyset$ 
5:    $obj_b \leftarrow \infty$ 
6:    $\text{phase}_0 \leftarrow 1$ 
7:    $\text{stay} \leftarrow \text{True}$ 
8:   for  $t = 0, 1, 2, \dots, T_{max}$  do
9:      $\mathcal{R}_{t,\text{total}}, \mathcal{S}_{t+1}, \mathbf{x}_b, obj_b \leftarrow \text{search}(M, \pi_\theta, \mathcal{S}_t, \mathbf{x}_b, obj_b, \text{phase}_t)$            {See Algorithm 1}
10:    if  $\text{stay} = \text{True}$  and ( $\mathbf{x}_{t+1} \in \mathcal{F}$  or  $t = T_{stay}$ ) then
11:       $\mathcal{S}_{t+1} \leftarrow \mathcal{S}_0$ 
12:       $\mathbf{x}_b \leftarrow \emptyset$ 
13:       $obj_b \leftarrow \infty$ 
14:       $\text{stay} \leftarrow \text{False}$ 
15:    else if  $\text{stay} = \text{False}$  and  $\mathbf{x}_{t+1} \in \mathcal{F}$  then
16:       $\text{phase}_{t+1} \leftarrow 2$ 
17:    end if
18:     $\delta_{td} \leftarrow \mathcal{R}_{t,\text{total}} + \gamma \cdot V_\theta(\mathcal{S}_{t+1}, \text{phase}_{t+1}) - V_\theta(\mathcal{S}_t, \text{phase}_t)$ 
19:     $\mathcal{L}_\theta \leftarrow -\log \pi_\theta(\mathcal{A}_t \mid \mathcal{S}_t, \text{phase}_t) \cdot \delta_{td} + \delta_{td}^2$ 
20:     $\theta \leftarrow \text{update}(\mathcal{L}_\theta, \theta)$ 
21:  end for
22: end for
23: return  $\theta$ 

```

D Pseudo-code for variable selection

Algorithm 3 Variable selection

Input: instance M , observation $\mathcal{S}_t = (\mathbf{x}_t, \mathbf{f}_t, obj_t)$, current phase $phase$

Parameter: number of seed variables p , number of neighboring variables q

Output: observation with selected variables $\tilde{\mathcal{S}}_t = (\tilde{\mathbf{x}}_t, \tilde{\mathbf{f}}_t, obj_t)$

```

1:  $\tilde{\mathbf{A}} \leftarrow \mathbb{I}(\mathbf{A}_{j,i} \neq 0)_{j=1,\dots,m; i=1,\dots,n}$ 
2: if  $phase = 1$  then
3:    $\tilde{\mathbf{f}}_t \leftarrow \mathbb{I}(f_{t,j} < 0)_{j=1,\dots,m}$ 
4:    $score\_seed \leftarrow \tilde{\mathbf{f}}_t^\top \tilde{\mathbf{A}}$   $\{\tilde{\mathbf{f}}_t \in \mathbb{R}^{m \times 1}, \tilde{\mathbf{A}} \in \mathbb{R}^{m \times n}\}$ 
5:    $weight \leftarrow (\max(\text{abs}(\mathbf{c}^\top)) - \text{abs}(\mathbf{c}^\top) + 1) / \max(\text{abs}(\mathbf{c}^\top))$ 
6: else if  $phase = 2$  then
7:    $\tilde{\mathbf{f}}_t \leftarrow \mathbb{I}(f_{t,j} > 0)_{j=1,\dots,m}$   $\{\tilde{\mathbf{f}}_t \in \mathbb{R}^{m \times 1}, \tilde{\mathbf{A}} \in \mathbb{R}^{m \times n}\}$ 
8:    $score\_seed \leftarrow \tilde{\mathbf{f}}_t^\top \tilde{\mathbf{A}}$ 
9:    $score\_seed \leftarrow \max(score\_seed) - score\_seed + 1$ 
10:   $weight \leftarrow \text{abs}(\mathbf{c}^\top) / \max(\text{abs}(\mathbf{c}^\top))$ 
11: end if
12:  $score\_seed \leftarrow score\_seed \odot weight$   $\{score\_seed \in \mathbb{R}^{1 \times n}\}$ 
13:  $prob \leftarrow score\_seed / \text{sum}(score\_seed)$   $\{prob \in \mathbb{R}^{1 \times n}\}$ 
14:  $indices\_seed \leftarrow \text{sample}(prob, p)$   $\{\text{Sample } p \text{ seed variables according to prob}\}$ 
15:  $\mathbf{g} \leftarrow \text{rowwise\_sum}(\tilde{\mathbf{A}}[:, indices\_seed])$   $\{\mathbf{g} \in \mathbb{R}^{m \times 1}\}$ 
16:  $score\_neighbor \leftarrow \mathbf{g}^\top \tilde{\mathbf{A}}$   $\{score\_neighbor \in \mathbb{R}^{1 \times n}\}$ 
17:  $score\_neighbor[:, indices\_seed] \leftarrow -1$   $\{\text{Prevent to select seed variables}\}$ 
18:  $indices\_neighbor \leftarrow \text{top}(score\_neighbor, q)$   $\{\text{Obtain top } q \text{ neighboring variables}\}$ 
19:  $changeable \leftarrow \text{concatenate}(indices\_seed, indices\_neighbor)$ 
20:  $\tilde{\mathbf{x}}_t \leftarrow \mathbf{x}_t[changeable]$   $\{\text{Select } \tilde{n} = p + q \text{ variables}\}$ 
21:  $\tilde{\mathcal{S}}_t \leftarrow (\tilde{\mathbf{x}}_t, \tilde{\mathbf{f}}_t, obj_t)$ 
22: return  $\tilde{\mathcal{S}}_t$ 

```

E Details of experimental setup

E.1 Benchmark datasets

Table 4 shows the average sizes of each benchmark dataset used in our experiments.

Table 4: Average sizes of each dataset.

Dataset	# binary variables	# integer variables	# constraints	Density
Independent set (IS)	1,500	0	5,962	0.13%
Combinatorial auction (CA)	4,000	0	2,715	0.21%
Set covering (SC)	3,000	0	2,000	5%
Minimum vertex cover (MVC)	3,000	0	11,931	0.07%
Non-binary integers (NBI)	0	2,000	2,000	10%

We generated instances for IS, CA, SC, and MVC following the code¹ from (Gasse et al., 2019). For NBI, instances were generated based on the description in (Qi et al., 2021). Table 5 summarizes the parameters used for NBI instance generation. Considering that the ratio of non-zero coefficients ρ in typical LP problems is less than 5% (Hillier & Lieberman, 2015), we set a higher density of 10% to promote more interactions between variables in constraints. According to the default settings of the ILP solver Gurobi (Gurobi Optimization, 2025) and SCIP (Bestuzheva et al., 2021), the lower bound l_i and upper bound u_i for decision variables are set to 0 and ∞ , respectively.

Table 5: Parameters for non-binary integer instance generation.

Parameter	Distribution
\mathbf{c}	randint[−10, 1]
\mathbf{A}	randint[1, 10] with density $\rho = 0.1$
\mathbf{b}	$\mathbf{A}\xi + \epsilon$, where $\xi_i \sim \text{randint}[1, 10], \forall i = 1, \dots, n$ and $\epsilon_j \sim \text{randint}[1, 10], \forall j = 1, \dots, m$
l_i	0, $\forall i = 1, \dots, n$
u_i	$\infty, \forall i = 1, \dots, n$

E.2 Evaluation environment

We conducted all evaluations under identical configurations. The evaluation machine is equipped with two AMD EPYC 7302 @ 3.0GHz, 2048GB RAM, and four NVIDIA A100 GPUs. All experiments were performed using a single NVIDIA A100 GPU. The software environment includes PyTorch 1.12.0, Gymnasium 0.29.1, and SCIP 8.1.0.

E.3 Implementation details

Our proposed model is implemented using the Transformer encoder code from GitHub² (Wu et al., 2021b), maintaining the same configuration. We utilized the positional encoding module from GitHub³ (Gorishniy et al., 2022). Our RL algorithm is built upon the Actor-Critic implementation in PyTorch⁴ (Kostrikov, 2018), modified to be tailored for ILP. The agent of RL-SPH was trained using the proposed learning algorithm (Algorithm 2) with RMSprop (learning rate = 1e-4, epsilon = 1e-5, alpha = 0.99, weight decay = 1e-3). The learning rate was linearly decayed over the training epochs. The agent of RL-SPH was trained concurrently on 64 different instances using the parameters for Algorithm 2 and Algorithm 3 as follows: update limit $N = 5000$, total step limit $T_{max} = 2000$, step

¹<https://github.com/ds4dm/learn2branch>

²<https://github.com/ucbrise/graphtrans>

³<https://github.com/yandex-research/rtdl-num-embeddings>

⁴<https://github.com/ikostrikov/pytorch-a2c-ppo-acktr-gail>

limit for *phase1* $T_{stay} = 500$, number of seed variables $p = \log_2 n$, and number of neighboring variables $p = \log_2 n$. With $N = 5000$, the training times for IS, CA, SC, MVC, and NBI were approximately 31, 32, 26, 83, and 23 minutes as shown in Table 6, respectively. We used the code for PAS (Han et al., 2023), which is available on GitHub⁵.

Table 6: Training time of the agent of RL-SPH on each dataset.

Dataset	IS	CA	SC	MVC	NBI
Training time (min)	31	32	26	83	23

F Impact of toward-optimal bias

Table 7 shows the impact of the toward optimal bias α . With a toward-optimal bias (i.e., $\alpha = 2$), RL-SPH tends to find better solutions than those without the toward-optimal bias (i.e., $\alpha = 1$). The trained agent chooses the lesser of two evils, as the potential penalty for solutions with $obj_{t+1} < obj_b$ is lower than for those with $obj_{t+1} \geq obj_b$ (see Appendix B.3). A suitable toward-optimal bias promotes exploration toward better feasible solutions with $obj_{t+1} < obj_b$, enhancing solution quality. This highlights the importance of guiding the agent’s search.

Table 7: The impact of the toward-optimal bias on Performance in terms of FR, PG, PI and #win, where #win measures the number of test instances where a method reaches the best value obtained among all compared methods. In case of a tie, each method receives a count for #win.

Dataset	Toward-optimal bias	FR (%) \uparrow	PG (%) \downarrow	PI \downarrow	#win
IS	✗	100	4.31 \pm 2.30	7.6 \pm 1.1	2
	✓	100	0.05 $^{+0.36}_{-0.05}$	3.6 \pm 0.3	98
CA	✗	100	2.82 $^{+3.05}_{-2.82}$	12.3 \pm 1.4	25
	✓	100	0.47 $^{+1.36}_{-0.47}$	11.7 \pm 1.1	75
SC	✗	100	1.41 $^{+1.93}_{-1.41}$	97.7 \pm 7.1	54
	✓	100	1.46 $^{+2.23}_{-1.46}$	97.9 \pm 8.3	61
MVC	✗	100	13.80 \pm 1.06	8.6 \pm 0.5	0
	✓	100	0.00 \pm 0.00	4.4 \pm 0.2	100
NBI	✗	100	0.18 \pm 0.11	10.9 \pm 0.6	5
	✓	100	0.00 $^{+0.02}_{-0.00}$	10.8 \pm 0.7	95

⁵https://github.com/sribdcn/Predict-and-Search_MILP_method